NRIAG Journal of Astronomy and Geophysics (2012) 1, 23–32

National Research Institute of Astronomy and Geophysics

NRIAG Journal of Astronomy and Geophysics

www.elsevier.com/locate/nrjag

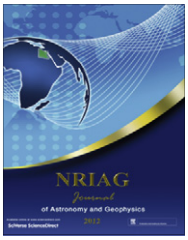

FULL LENGTH ARTICLE

Application of ERT and SSR to detect the subsurface cave at 15th May City, Helwan, Egypt

A.A. Basheer [a,*], M.A. Atya [a], M. Shokri [b], M.M. Abu shady [a]

[a] National Research Institute of Astronomy and Geophysics (NRIAG), Helwan, Cairo, Egypt
[b] Geophysics Department, Ain Shams University, Cairo, Egypt

Received 15 October 2012; accepted 20 November 2012
Available online 20 January 2013

Abstract 15th May City, 12 km to the southeast of Helwan city, is one of promised cities planned in 1986 by the Egyptian government through its program to withdraw the population from the condensed central Nile valley to the side parts of the Nile valley Egypt.

The present study runs on the famous and known place of the city that is called "the cave". The main target of this study is to detect the nearly shape of this cave and estimate its extension and dimension parameters. This study embraces, two dimension electrical resistivity, and shallow seismic refraction surveys.

The two dimension electrical imaging technique was interpreted in terms of depths and thicknesses of the geoelectric layers, on this regard, it suggests a succession of one to two layers, and in addition, the boundaries of the cave could be sensed. The shallow seismic refraction technique results revealed a succession of one to two seismic layers. These layers illustrated from both techniques are limestone "calcite to dolomite" layer, and the second layer "fractured limestone". On the other hand, these parameters allow for separating the area into parts of different competence nature and consequently different appropriateness, and stand to detect and draw the boundaries of the cave underground.

Finally, it is outstanding to mention that, within the investigated depth of seismic profiles, their interpreted layers are in close agreement with both shape and thickness of the interpreted layers from the R2D sections and this chains the results obtained from both techniques especially in the geotechnical survey.

* Corresponding author. Tel.: +20 1122802222.
E-mail address: Alhussein007@yahoo.com (A.A. Basheer).

Peer review under responsibility of National Research Institute of Astronomy and Geophysics.

Production and hosting by Elsevier

Introduction

The 15th May City is one of the new residential cities. The study area covers an area of about 1200 m^2. It is portrayed between latitudes 29°50′9″ and 29°50′11″N and longitudes 31°22′25″ and 29°22′31″E (Fig. 1). The city, as a residential one, has heavy

2090-9977 © 2012 National Research Institute of Astronomy and Geophysics. Production and hosting by Elsevier B.V. All rights reserved.
http://dx.doi.org/10.1016/j.nrjag.2012.11.003

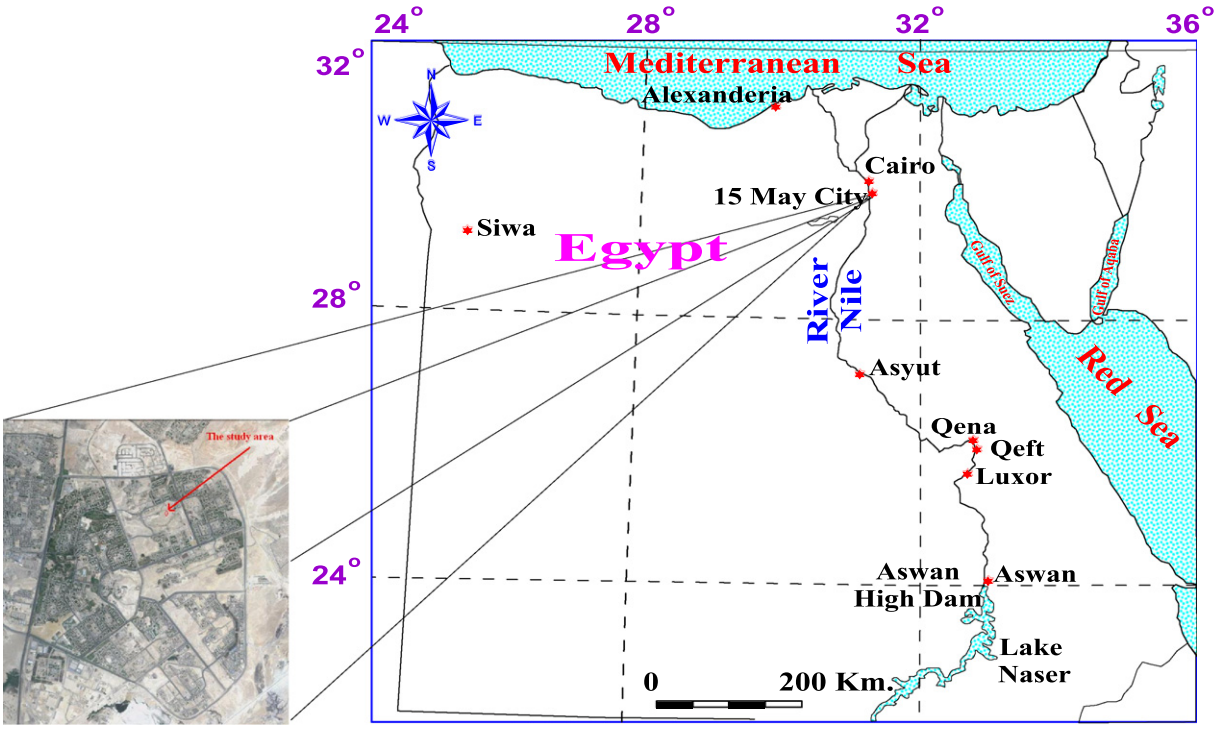

Fig. 1 Location map of the study area.

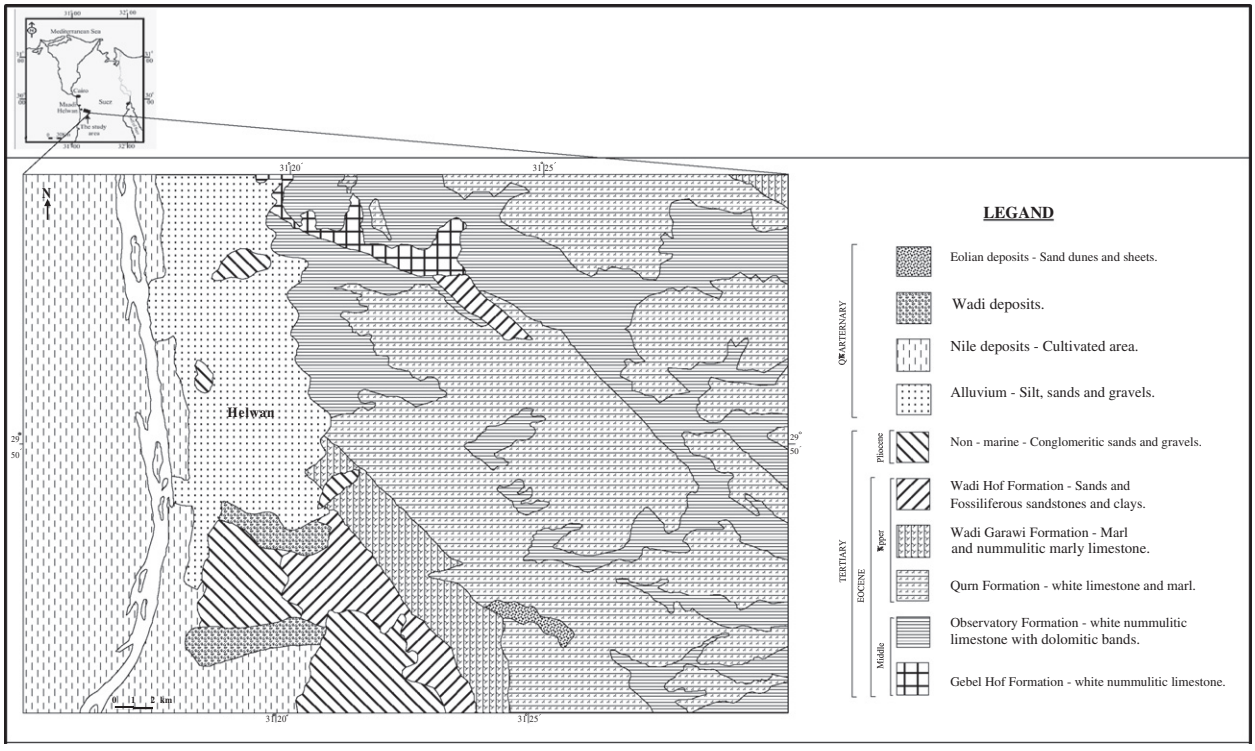

Fig. 2 Geologic map of 15th May area, compiled from the Geological Survey of Egypt (1983) and Conoco Coral (1987).

constructions either for the factories or worker housings and also continuous motive heavy trucks. Therefore, a careful study is undoubtedly required to outline the subsurface fittingness for constructing heavy load roads and construction building.

15th May City utilized both of the two dimension electrical array "R2D" and Shallow Seismic Refraction "SSR" surveys. Most possibly, it will aid in the location of any probable interrupted caves, structural features, and is capable of furnishing

Table 1 Eocene rock units of G. Mokattam and east of Helwan (modified from Strougo, 1979; Moustafa et al., 1985).

Age	G. Mokattam	Area east of Helwan
Late Eocene	Anqabia formation	Wadi Hof series
	Maadi formation	Wadi Garawi series
		El-Qurn series
Middle Eocene	Mokattam formation	Observatory series
		G. Hof series

useful information to detect the characterization of the nature of the foundation materials. According to the geometry of the wave propagation in the earth, the measuring techniques could be classified into reflection and refraction. Seismic refraction method is the most widely applied as a reconnaissance tool in newly explored areas, especially in engineering projects. It mostly used in the mapping of the layers at shallow depth, layer thicknesses and some data about lithology can be obtained.

The integrated interpretation of the both techniques classified the subsurface into two layers. They gave also interesting information about the geotechnical competent of the ground and some key control to the structure feature.

Geological setting

Surface geology

The geology of Helwan area in general and 15th May city especially was discussed by Awad et al. (1953), Shukri (1953), Said (1962, 1971), Farag and Ismail (1955, 1959), Ismail and Farag (1960), Moustafa et al. (1985), and Strougo (1976, 1979). These studies, with field observations of the author, represent the bases of the discussion around the study area; that touches the geology, the geomorphology, stratigraphy, and the structure. Fig. 2 is the geologic map of the area east Helwan including the study area.

Stratigraphy

The stratigraphic units at some localities of the study area were studied by Cuvillier (1924a,b, 1930), Awad et al. (1953), Shukri (1953), Farag and Ismail (1955), Ismail and Farag (1960), Said (1962, 1971), Tadros (1968), Ghobrial (1971), Strougo (1976, 1979), and Moustafa et al. (1985). Middle Eocene, Upper Eocene, and Oligocene rocks crop out in the mapped area. Several

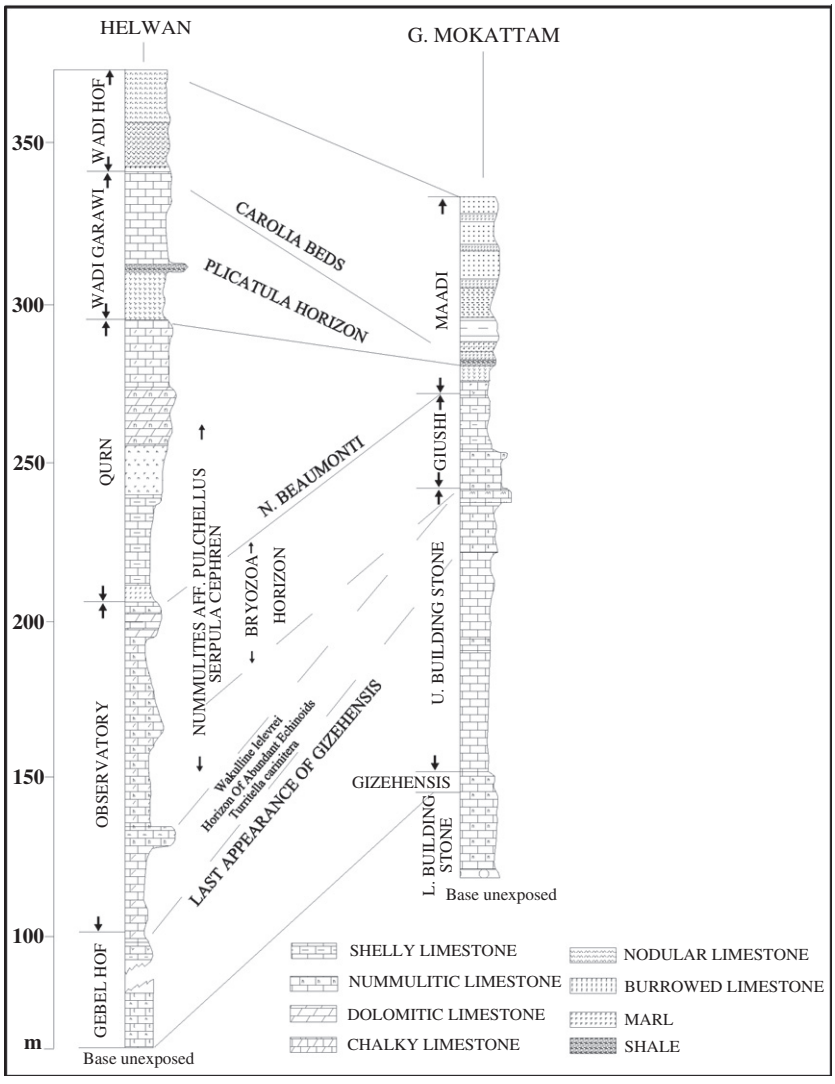

Fig. 3 Helwan area lithologic sections; data from Strougo, 1976.

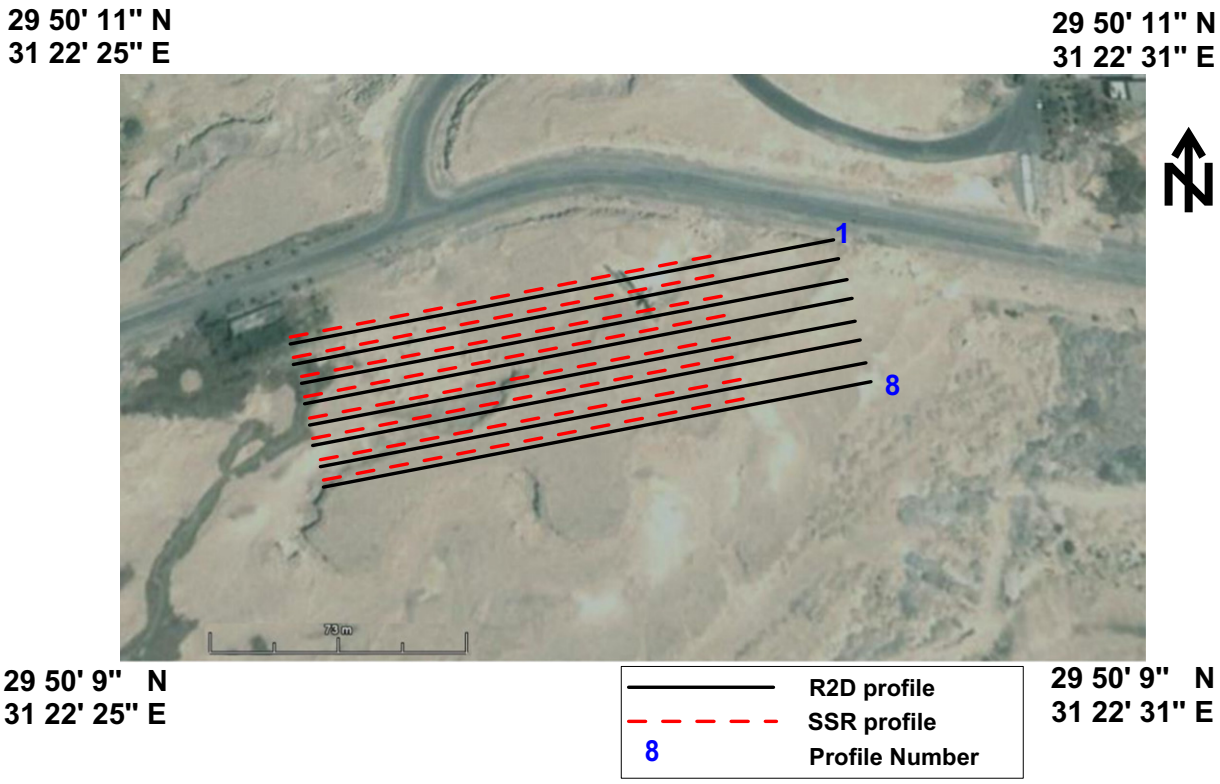

Fig. 4 Location map of the study area shows R2D and SSR profiles.

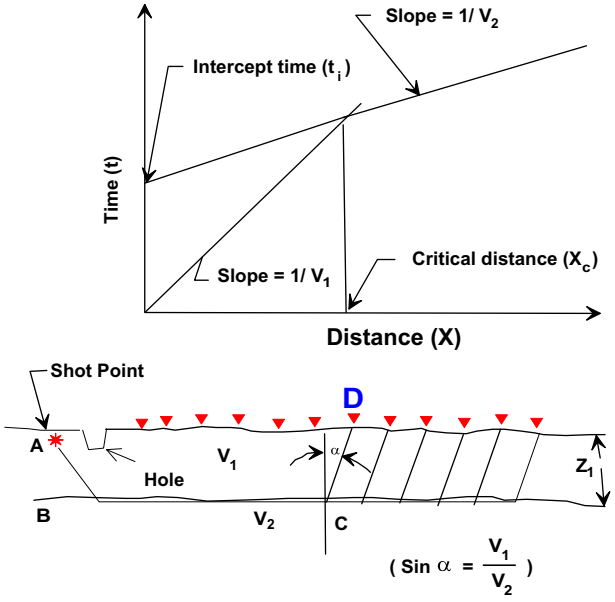

Fig. 5 Velocity estimation using the slope method calculation with shot point and geophones array in field (after Basheer, 2003).

classifications were proposed for the Eocene rocks in the different parts of the study area. Table 1 shows the most-accepted classifications of G. Mokattam and the area east of Helwan.

Nine stratigraphic sections were drawn in different parts of the study area (Fig. 3). They are correlated, based on lithologic and faunal similarities, in order to have only one set of rock units that can used in every part of the study area and also to be used for constructing the geologic map.

A brief description of the mapped rock units with their thicknesses is given below, considering the maximum thickness for all units. The detailed description of these units is given as follows (Strougo, 1976; Moustafa et al. 1985).

Data acquisition

R2D electrical imaging survey

The utmost constraint of the resistivity sounding method is that it does not take into description horizontal changes in the subsurface resistivity. The 2-D imaging survey conquers this problem, where the resistivity changes in the horizontal direction as well as in the vertical direction along the survey line. Therefore, the 2-D geo-electrical imaging technique was selected for the survey. While, the Wenner array gives the smallest number of possible measurements compared to the other common arrays (Griffiths and Barker, 1993), also it competent to work in noisy fields and when good vertical resolution is required. The Wenner array has been used in the present work.

The geo-electrical data obtained along eight profiles, of 147 m length, distributed over the study area (Fig. 4). The survey has been accomplished using a 48 multi-electrodes system connected to SYSCAL R2 resistivity meter through a multicore cable. A built-in microcomputer together with an electronic switching unit is used to automatically select the relevant four electrodes for each measurement.

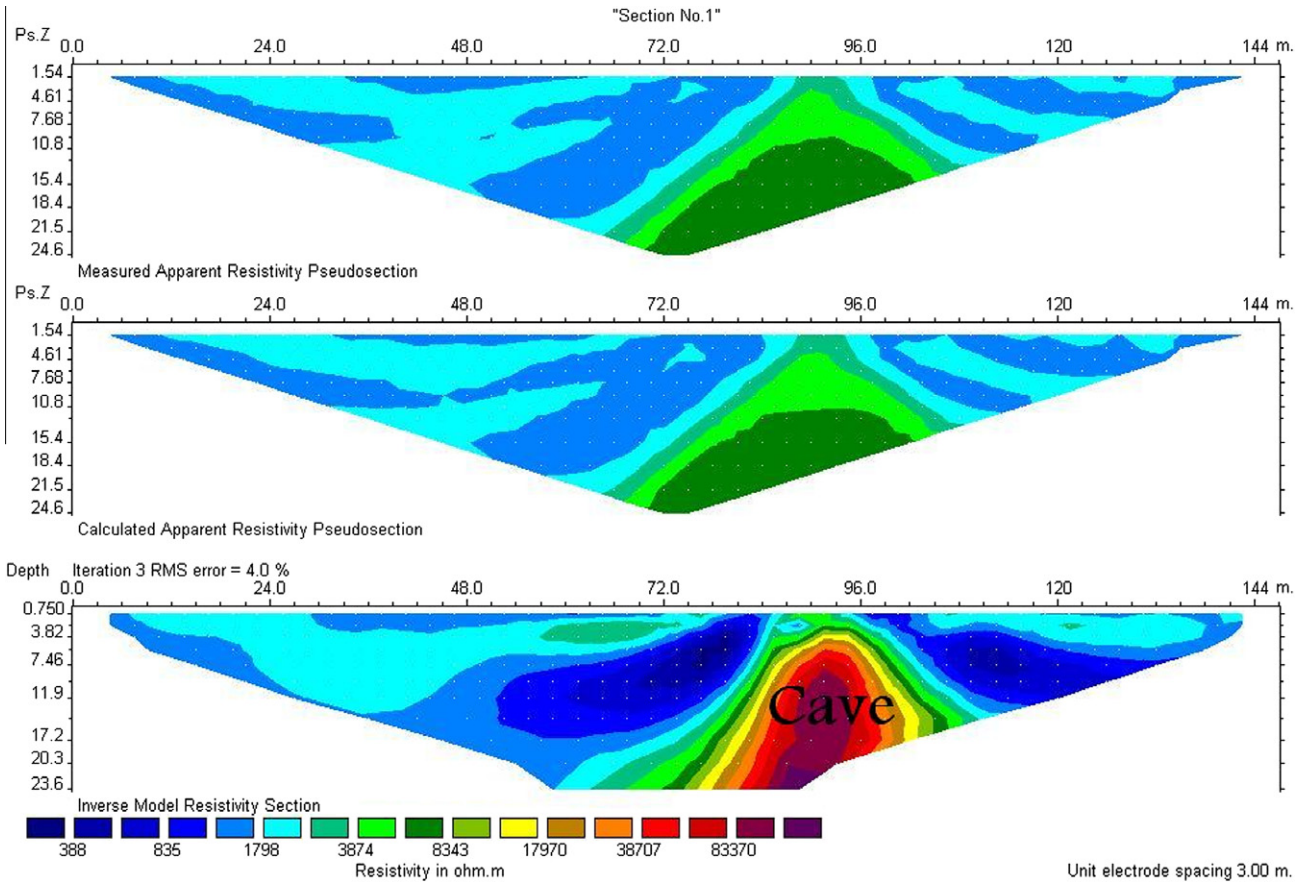

Fig. 6 R2D Geoelectrical cross section along profile No. 1.

Seismic survey

Seismic exploration involves generation of seismic waves and recording the arrival times of these waves from the source to the series of geophones (Dobrin, 1976). Seismic refraction is used to evaluate the necessary parameters for constructions, or to solve the problems related to the geologic nature of sub-surfaces, mining works, and the environmental conditions overcame in the site (Sharma, 1974; Dutta, 1984).

The seismic refraction data has been acquired along eight shallow seismic refraction profiles spread over the same area proposed for the R2D resistivity imaging survey. The survey has been accomplished using 24 channels signal enhancement seismograph ''GEOMETRICS SMARTSEIS'' along 120 m length profiles (Fig. 4). In the surface P and SH wave velocities have been specified. The hammer connects to sensor to provide the time break to the seismograph. The power of the hammer helping to avoid loosing of waves strength that may cause by Blind layer in some condition. The low pass filter in the recording system has 7–10 MHz as frequency response, which is suitable for the recording condition, positioned before the analog–digital conversion circuit. Some special arrangement has done to create and detect un-noisy SH-wave in the field (Fig. 5), first step was to switch the vibration generator to SH-wave position ''To pulse in 45° angle'' in the shot point position, second step was to make hole between the first geophone and the shot point, this hole make the P-waves, which certainly will be created with SH-waves, deploy in very high distributed material ''air''. P-waves will be delayed and weak, so the most waves reach geophones will be SH-waves and geophones can only detect the SH-wave. On the other hand, the SH-waves less in values than P-waves, so it can be digitally separated by software program.

Data interpretation

Geo-electrical imaging R2D

The resistivity data was interpreted by using RES2DIN RES2DINV software, edited in 1998, (Loke, 2000, 2002) to estimate:

(1) The different layer parameters such as (depth, and resistivity under each electrode).
(2) The electric cross sections along each recorded profile in the study area.

According to the general view up of the constructed cross sections, two layers could be defined in the study area. The surface layer consists of very dry and weathered limestone. The second layer lies under the surface layer and it consists of fractured limestone. This layer appears as dotted layer with very high resistivity related to fractures in layer which filled up by air. Fig. 7 shows the geoelectric cross section constructed over profile No. 8 as an example for this area. The third feature is classified as the cave; it can be noted as very high resistivities

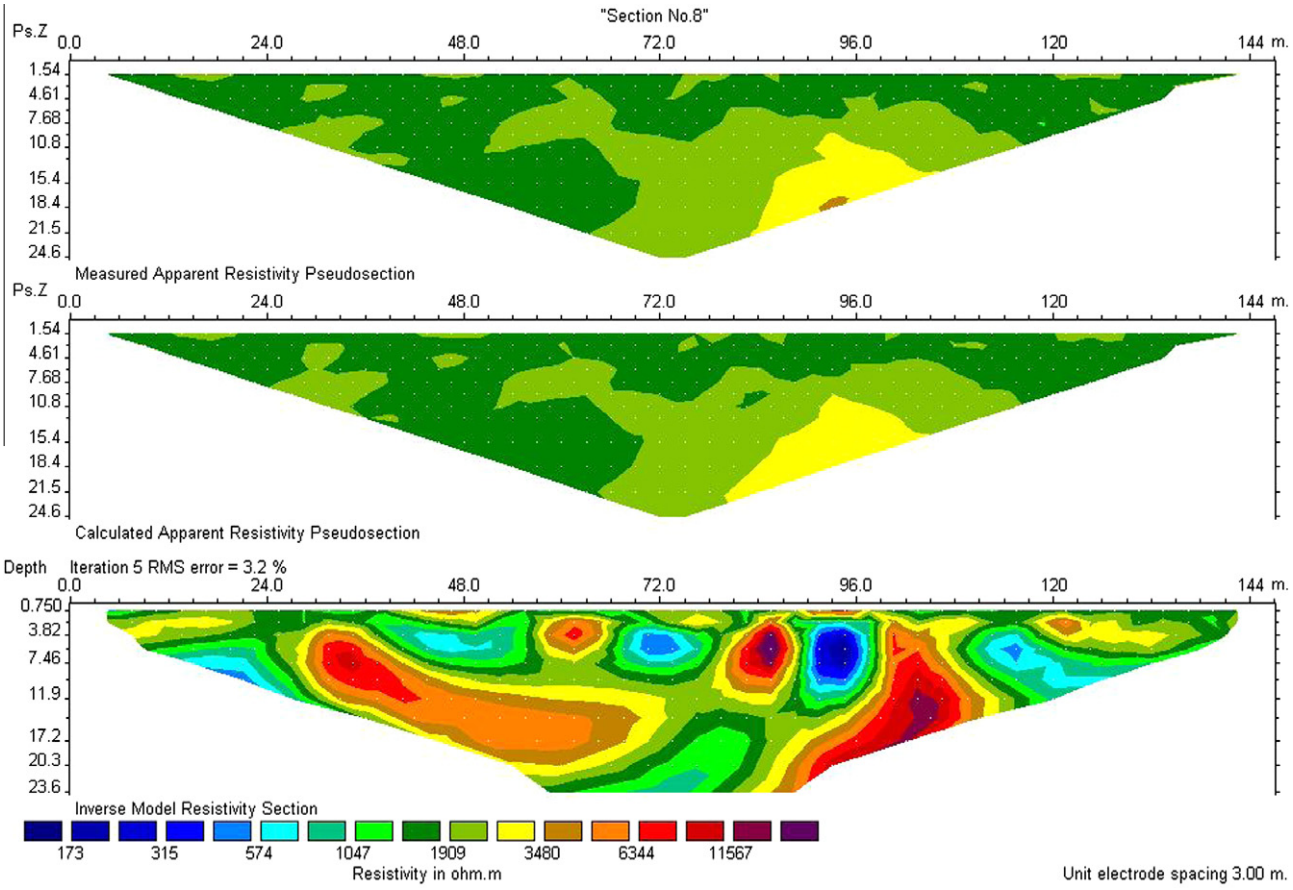

Fig. 7 R2D Geoelectrical cross section along profile No. 8.

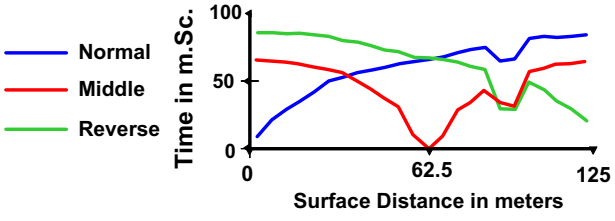

Fig. 8 Time–distance curves along profile No. 1.

values. The effects of the cave extended to the second layer around it. Fig. 6 shows the geoelectric cross section No. 1 over the cave and its effects.

SSR data interpretation and discussion

The data has been treated using a computer program called SEIPEEDIT (2002) to construct the travel time curve, in which the time of the first arrival is plotted versus the geophone offset distance. The time of the first arrival and its velocity are functions of the depth of the refracted interface according to the equation:

$$V = D/T \tag{1}$$

while V is the velocity, D is the offset distance (the distance between shot point and the detected geophone), and T is the time that wave take from shot point to geophone.

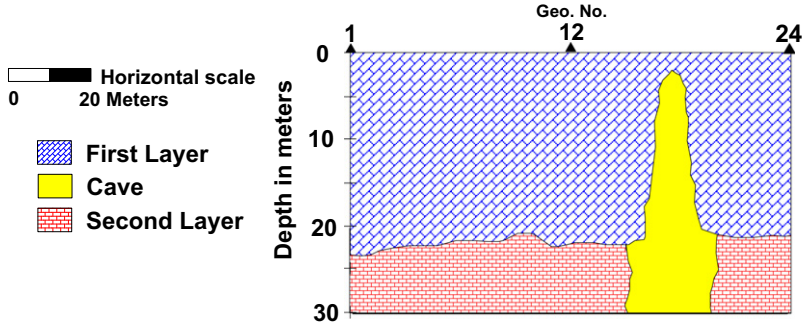

Fig. 9 The lithological layers interpreted from the seismic data of the profile No. 1.

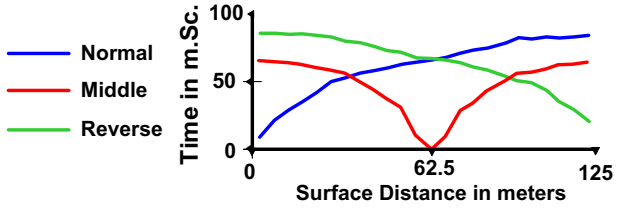

Fig. 10 Time–distance curves along profile No. 8.

The layer's parameters (thickness, depths, and the different velocities under each geophone) have been estimated and used to construct geoseismic cross sections (Fig. 5).

Seismic velocity in a geologic material is related to the low-strain dynamic modulus of the material. Soil modulus is influenced by density, confinement and cementation. Consequently, P-wave seismic velocity in a soil mass is influenced by density, confinement and cementation. Relationships between density, overburden pressure and modulus in limestone, and fractured limestone have been studied and refined since at least the 1960s. One of the older relationships that results in velocity change of cohesionless soil with depth, based on changes in soil modulus that scale to the square root of the effective stress at a given soil density (Richart et al., 1970), is presented in Figs. 12–17. The interpreted vertical velocity gradient presented in these figures matches very closely with that cohesionless soil relationship. Cohesionless material modulus manifested as seismic velocity is significantly controlled by the effective stress manifested as overburden pressure at subsurface depth. Soil losing is lessening material strength, and thus modulus decreased, at least partly independent of overburden pressure and subsurface depth. At shallow depths with relatively little-overburden pressure, loosation and variability can result in lower seismic velocities than would occur without variability. Seismic velocity at shallow depths can thus become an interpretation for the presence of variability and cementation (Rucker, 2000).

It is important to mention that the most interpretation for profiles depended on the profiles done on the normal and middle shooting position and compares it with the reverse ones. It releases to avoid the confused data and output signals caused from Blind layer "The cave" that contain air which absorbed and weak waves.

The inspection of the constructed seismic cross sections could lead to the same result similar to the R2D results. The study area can be classified to two zones, the first zone consists of two seismic layers with much observed cave feature could be noticed over the seismic lines from 1 to 6. Figs. 8 and 9 represent the time–distance curve and the interpretive lithological

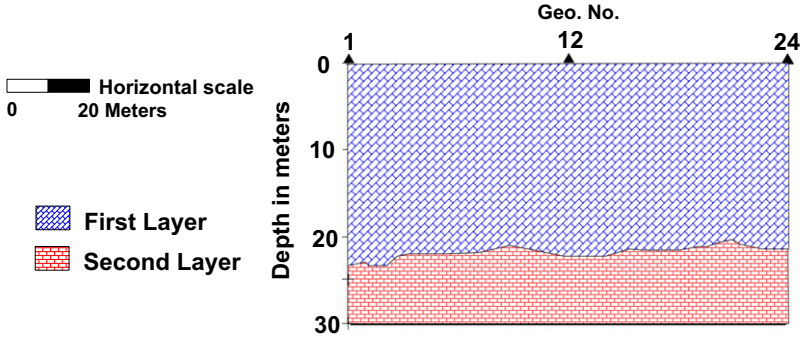

Fig. 11 The lithological layers interpreted from the seismic data of the profile No. 8.

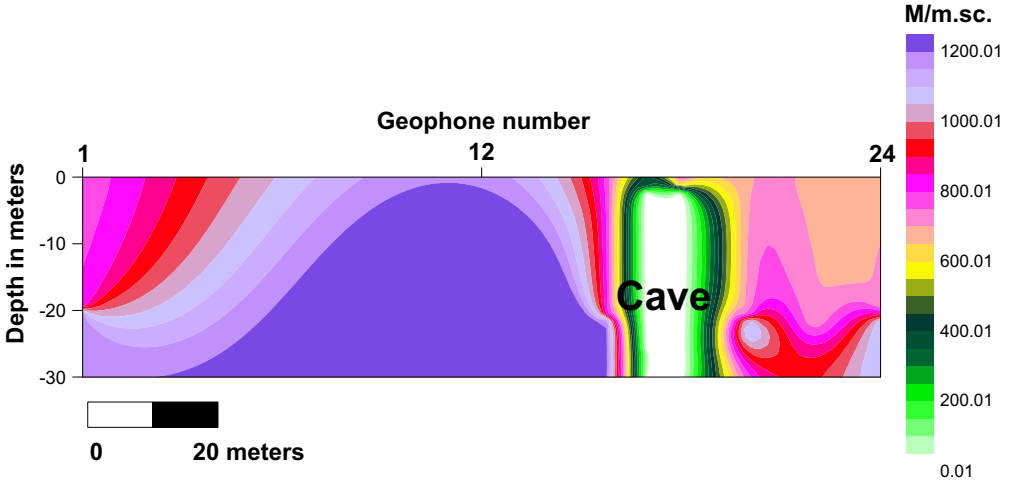

Fig. 12 The P-waves distribution along profile No. 1.

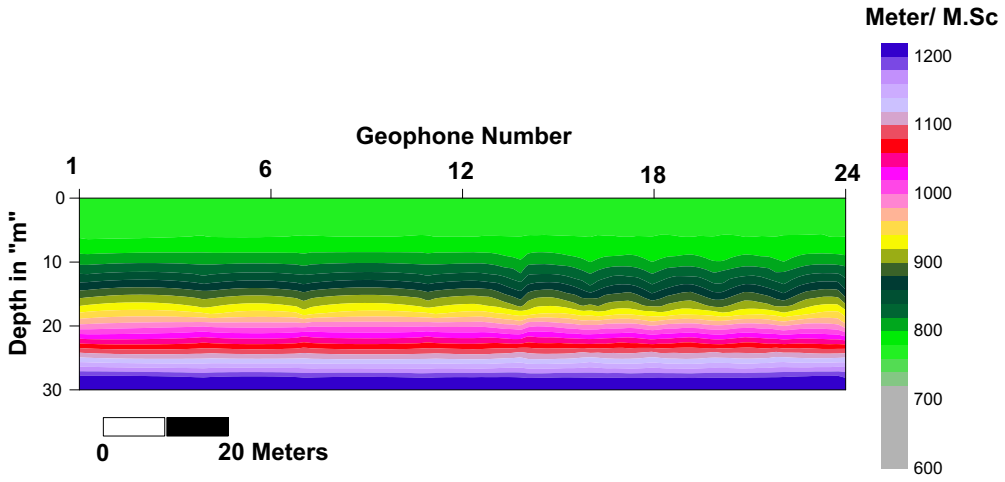

Fig. 13 The P-waves distribution along profile No. 8.

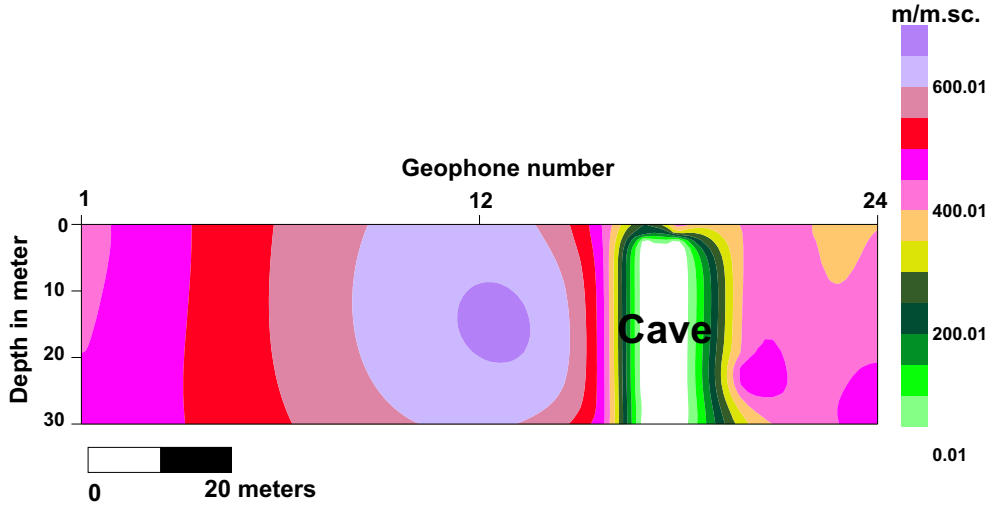

Fig. 14 The SH-waves distribution along profile No. 1.

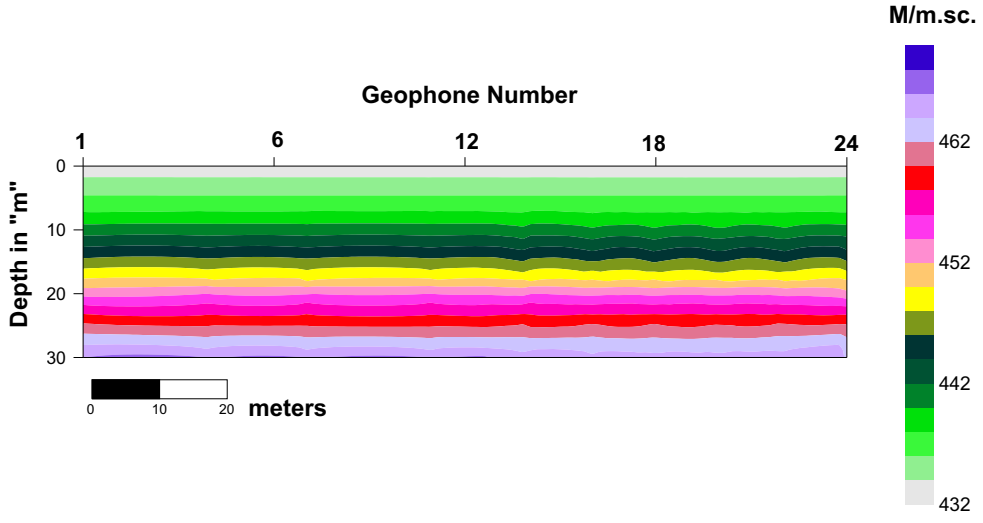

Fig. 15 The SH-waves distribution along profile No. 8.

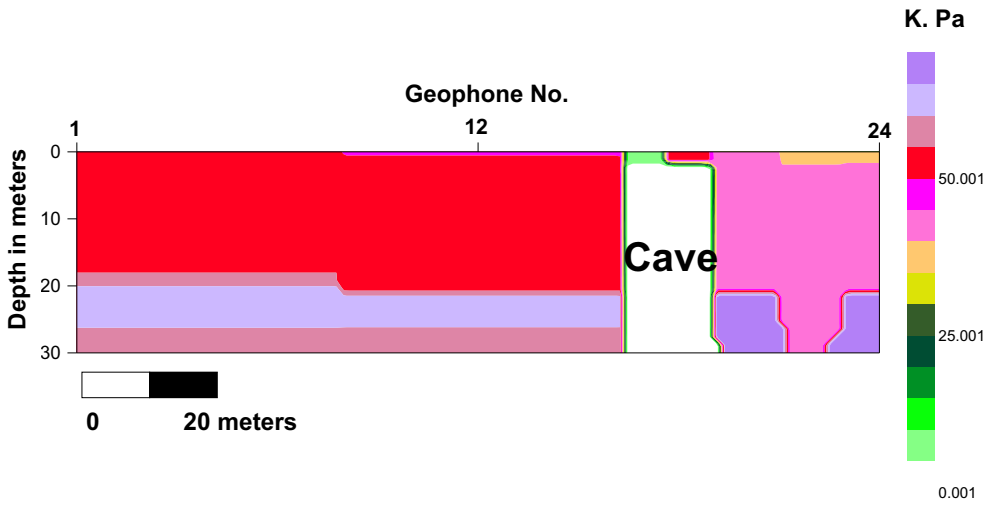

Fig. 16 The distribution of the allowable bearing capacity (Qa) along profile No. 1.

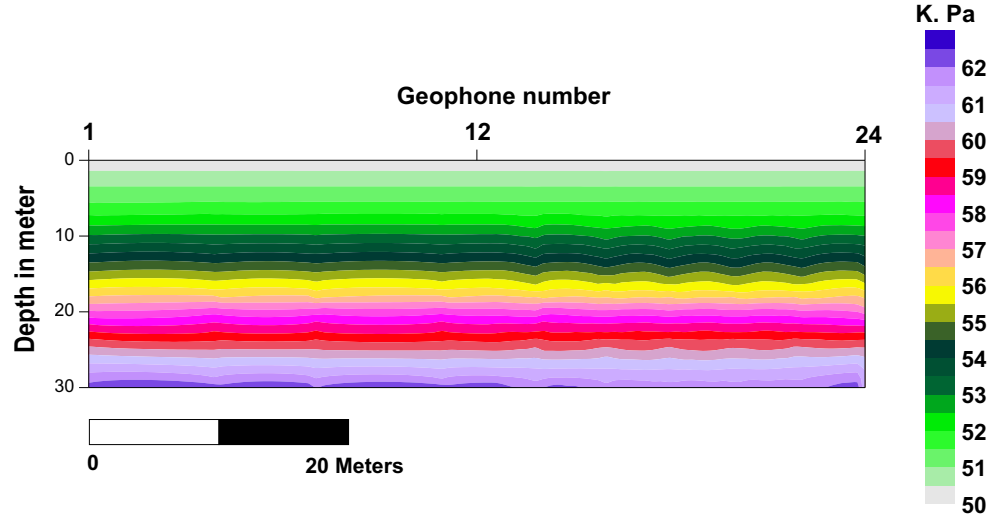

Fig. 17 The distribution of the allowable bearing capacity (Qa) along profile No. 8.

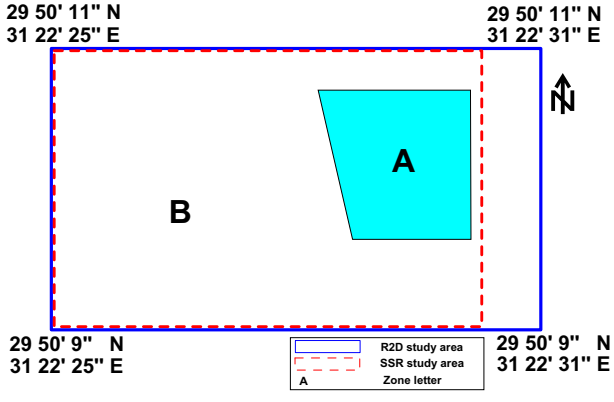

Fig. 18 The studied area classified into two zones; Zone A is the cave area, and Zone B is the normal lithology.

reading respectively of profiles 1 and 8 as examples of these lines. The same result for this zone could be noted too in Figs. 12, 14 and 16 shows (P-wave velocity, SH-wave velocity, and allowable bearing capacity "Qa"). The second zone consists of the same two seismic layers but with no presence of the cave feature, this zone could be seen over the rest of the measuring lines. Figs. 10 and 11 represent the time–distance curve and lithological interpretation respectively as an example of the second zone. Figs. 13, 15 and 17 show the vertical distribution of (P-wave velocity, SH-wave velocity, and allowable bearing capacity "Qa") for profile No. 8 as an example of the same zone.

Finally, a comprehensive interpretation of the R2D and the SSR data could lead to define two lateral zones (Fig. 18); the first zone marked as Zone A; it occupies the northeastern quarter of the area and represents edges of the subsurface cave. This zone is not suitable at all for any construction extensions. The second zone is marked as Zone B and is laid at the rest portions of the study area. The materials at this zone are relatively competent but the ground is not suitable for constructions and engineering purposes because the second layer

consist of fractured limestone which is very unstable material to bear load or human activities.

Summary and conclusions

The present study has been conducted mainly to detect the site of the cave and provide an interpretation of the data in terms of the foundation rock materials and parameters.

The study involves carrying out of two main geophysical techniques integrately; the first technique embrace executing 2D electrical resistivity imaging survey in the form of eight parallel profiles using the Wenner electrode arrangement with maximum spread of 147 m, 5 m between the electrodes and 10 m interline distance using the SYSCAL R2 system. The second technique of the study depends on the analysis of the seismic refraction data acquired using eight shallow seismic refraction profiles distributed over a suggested portion of the study area that contain cave. In the survey, the velocities of the P- and SH-wave have been specified. Most interpretation for seismic profiles has done on normal and middle shooting position type to avoid the effect of Blind layer that causes attenuation of waves. Through the R2D survey, the penetrated depth reached about 24 m while the penetrated depth reached with the SSR varied from 27 m under geophone No. 16 of profile 5 to 29.3 m under geophone 22 of profile 2.

The integrated results obtained from the interpretation of both of the R2D and the SSR records conducted over the suspected site in the study area could be classified lithologicaly into two zones; the first include two layers invaded with one structural feature as a subsurface cave, and the second includes the same model as the first zone with a cave (Fig. 18). These layers from the top to the bottom as follows:

(a) Top soil layer consists of weathered limestone; its thickness varies between about 20.2 m and about 23.12 m.
(b) Fractured limestone with thickness varies from 7.3 to 10.33 m.
(c) A cave, the dimensions of this cave could be estimated from some profiles within 5–20 m in width and 1.13–25 m in long. Sometimes, this layer invades between the 1st and the 2nd layers.

According to the lateral distribution of the lithological layers' parameters, the area could be zoned as follow:

(1) Zone A: this zone occupies the northeast quarter of the study area; it consists of a cave make the zone of less competent area with limited unsuitability for any construction extensions.
(2) Zone B: this zone covers the most study area. It consists of competent materials characters that suggest it unsuitable for any engineering purposes.

References

Awad, G.H., Faris, M.I., Abbas, H.L., 1953. Contribution to the stratigraphy of the Mokattam area east of Cairo. Bulletin de l'Institute du Desert d'Egypte 3 (2), 106–107.

Basheer, A.A., 2003. Application of Geophysical Techniques at New Qena City, Qena, Egypt. Master Degree in Geophysics, Faculty of Science in Qena, South Valley University.

Cuvillier, J., 1924a. A conglomerate in the Nummulitic formation of Gebel Mokattam, near Cairo. Geological Magazine 64, 522–523.

Cuvillier, J., 1924b. Contibution a l'etude geologique du Mokattam. Bulletin de l'Institute du Desert d'Egypte 6, 94–102.

Cuvillier, J., 1930. Revision du Nummilitique Egyptien. Mémoires présentés à l'Institut d'Egypte journal 16, 371.

Dobrin, M.B., 1976. Introduction to geophysical prospecting, 3rd ed. Mc Graw Hill Book C, New York, pp. 25–56, 292–336 and 568–620.

Dutta, N.P., 1984. Seismic refraction method to study the foundation rock of a dam. Geophysical Prospecting 32, 1103–1110.

Farag, I.A.M., Ismail, M.M., 1955. On the structure of the wadi Hof area (north-east of Helwan). Bulletin de l'Institute du Desert d'Egypte 5 (1), 179–192.

Farag, I.A.M., Ismail, M.M., 1959. Contribution to the stratigraphy of the wadi Hof area (north-east of Helwan). Bulletin of the Faculty of Science, Cairo University 34, 147–168.

Ghobrial, G.A., 1971. Geological studies in the area east of Maadi. M.Sc. Thesis, Cairo Univ., pp. 114.

Griffiths, D.H., Barker, R.D., 1993. Two-dimensional resistivity imaging and modeling in areas of complex geology. Journal of Applied Geophysics 29, 224–226.

Ismail, M.M., Farag, I.A.M., 1960. Contribution to the stratigraphy of the area east of Helwan (Egypte). Bulletin de l'Institute du Desert d'Egypte 7 (1), 95–134.

Loke, M.H., 2000. Electrical imaging surveys for environmental and engineering studies, A practical guide to 2-D and 3-D surveys. Available from: <https://pangea.stanford.edu/research/groups/sfmf/docs/DCResistivity_Notes2.pdf>.

Loke, M.H., 2002. 2-D and 3-D Electrical Imaging Surveys. Available from: <www.geoelectrical.com>.

Moustafa, A.R., El-Nahhas, F., Abdel Tawab, S., 1985. Structural Setting of the Area East of Cairo, vol. 5. Middle East Research Center, Ain Shams University Science Research Senr., Maadi, Helwan, pp. 40–64.

RES2DINV Program Version 3.55.49. Copyright (1995–2006) Geotomo software. Available from: <www.geoelectrical.com>.

Said, R., 1962. The Geology of Egypt. Elsevier Pub. Co., Amsterdam, pp. 377.

Said, R., 1971. Explanatory notes to accompany the geological map of Egypt. Geol. Survey Egypt 3 (2), 89–105 (Special paper No. 56, Cairo).

SEIPEEDIT Program Version 6.23, 2002. Seismic Interpretation Program Software, OHOO Company, New York. Available from: <www.Ohoo.com>.

Sharma, P.V., 1974. Geophysical Methods in Geology. Elsevier, New York, 428p.

Shukri, N.M., 1953. The geology of the desert east of Cairo. Bulletin de l'Institute du Desert d'Egypte 3 (2), 89–105.

Strougo, A., 1976. Decouverte d'une discontinuite de sedimentation dans l' Eocene superieur du Gebel Mokattam (Egypte). C. R. Somm. Séanc. Social Geology, France 5, 213–215.

Strougo, A., 1979. The Middle-Eocene-Upper-Eocene boundary in Egypt. Annals of the Geological Survey of Egypt 9, 454–469.

Tadros, S.F., 1968. Geologic, palentologic and economic studies on some rocks from Mokattam area. M.Sc. Thesis, Ain Shams Univ., pp. 244.